Effects of Bulkiness and Hydrophobicity of an Aliphatic Amino Acid in the Recognition Helix of the GAGA Zinc Finger on the Stability of the Hydrophobic Core and DNA Binding Affinity†

Muthu Dhanasekaran,‡ Shigeru Negi, Miki Imanishi, Michiko Suzuki, and Yukio Sugiura*

Faculty of Pharmaceutical Sciences, Doshisha Women's University, Koudo, Kyotanabe-Shi 610-0395, Japan, and Institute for Chemical Research, Kyoto University, Uji 611-0011, Japan

Received July 11, 2008; Revised Manuscript Received September 10, 2008

ABSTRACT: The GAGA factor of *Drosophila melanogaster* uses a single Cys_2His_2-type zinc finger for specific DNA binding. The conformation and DNA binding mode of the GAGA zinc finger are similar to those of other structurally characterized zinc fingers. In almost all Cys_2His_2-type zinc fingers, the fourth position of the DNA-recognizing helix is occupied by the Leu residue involved in the formation of the minimal hydrophobic core. However, no systematic study on the precise role of the Leu residue in the hydrophobic core formation and DNA binding function has been reported. In this study, the Leu residue is substituted with other aliphatic amino acids having different side chain lengths and hydrophobicities, namely, Ile, Val, Aib, and Ala. The metal binding properties were studied by UV−vis spectroscopy. The peptide conformations were examined by CD and NMR spectroscopies. Furthermore, the DNA binding ability was examined with a gel mobility shift assay. Though the Ile, Val, and Aib mutants exhibited conformations similar to those of the wild type, the DNA binding affinity decreased as the side chain length of the amino acid decreased. Interestingly, the Val mutant can bind to the cognate DNA, while Aib cannot, in spite of the similarity in their secondary structures based on the CD measurements. Variable-temperature NMR experiments clearly indicated differences in the stability of the hydrophobic core between the Val and Aib mutants. This study demonstrates that the bulkiness of the conserved aliphatic residue is important in the formation of the well-packed minimal hydrophobic core and proper ternary structure and that the hydrophobic core stabilization is apparently related to the DNA binding function of the GAGA zinc finger.

The classical Cys_2His_2-type zinc finger is the most common DNA-binding domain found in human transcription factors, and this domain constitutes 2% of the entire human genome (*1, 2*). In most cases, more than two zinc finger motifs in a tandem array are necessary for specific DNA binding (*1*). The GAGA transcription factor of *Drosophila melanogaster* is one of the typical Cys_2His_2-type zinc finger proteins (*3*). Different from other zinc finger proteins, the GAGA transcription factor has only one Cys_2His_2-type zinc finger motif as a DNA binding domain (GAGA-DBD),[1] and it binds to DNA derived from the h3/h4 promoter containing the sequence GAGAGAG (*4*). Therefore, the GAGA-DBD is a very attractive domain for the direct investigation of correlations between the zinc finger conformation and DNA binding function.

The GAGA zinc finger core is 26 residues in length and has a compact $\beta\beta\alpha$ fold stabilized by the tetrahedral coordination of Zn(II) with two Cys (C) and two His (H) residues similar to other structurally characterized zinc finger proteins (*5, 6*). A Cys_2His_2-type zinc finger motif typically recognizes a triplet of DNA base pairs via key amino acids located at positions −1, 3, and 6 in the "recognition helix" as seen in the X-ray structures of the DNA complexes of Tramtrack, Zif268, and GLI (*7*−*9*). Many research groups successfully exploited the recognition code details to customize the DNA specificity of a particular zinc finger (*10*−*12*). However, not many reports about the mutational effects of other positions apart from the DNA-contacting amino acids in the helical region are available.

In general, the classical Cys_2His_2-type zinc finger domain has conserved hydrophobic residues (typically, Tyr, Phe, and Leu) present in the β-hairpin and α-helix (*1, 7*−*9*). Previous studies have demonstrated that these hydrophobic residues cooperatively form a compact hydrophobic core which can be observed only when Zn(II) is present (*13*). Moreover, the

† This work was supported by a grant (17390028) from the Ministry of Education, Culture, Sports, Science, and Technology, Japan. M.D. was supported by a JSPS research fellowship from the Japan Society for the Promotion of Science.

* To whom correspondence should be addressed: Faculty of Pharmaceutical Sciences, Doshisha Women's University, Koudo, Kyotanabe-Shi 610-0395, Japan. Telephone: +81-774-8649. Fax: +81-774-8652. E-mail: ysugiura@dwc.doshisha.ac.jp.

‡ Present address: Department of Chemistry, University of Arizona, Tucson, AZ 85721.

[1] Abbreviations: aa, amino acid(s); CD, circular dichroism; DSS, 2,2-dimethyl-2-silapentane-5-sulfonate sodium salt; FITC, fluorescein isothiocyanate; Fmoc, 9-fluorenylmethoxycarbonyl; GAGA-DBD, GAGA DNA-binding domain; HATU, *O*-(7-azabenzotriazol-1-yl)-1,1,3,3-tetramethyluronium hexafluorophosphate; RP-HPLC, reversed-phase high-performance liquid chromatography; TMP, 2,4,6-trimethylpyridine (collidine); Tris, tris(hydroxymethyl)aminomethane; TB, tris-boric acid; UV−vis, ultraviolet−visible.

10.1021/bi801306d CCC: $40.75
Published on Web 10/15/2008

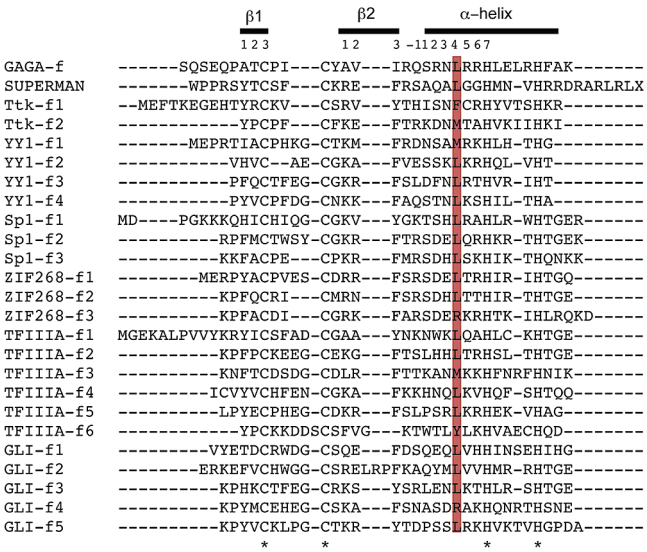

FIGURE 1: Sequence alignment of the GAGA zinc finger core with other selected structurally characterized zinc fingers having the general structure (F/Y)-X-C-X(2−4)-C-X(3)-(F/Y)-X(5)-L-X(2)-H-X(3−5)-H by BLAST. Zn(II) binding residues (Cys and His) are denoted with an asterisk. The positions of the DNA recognition helix and two β-strands are indicated by the position numbering within them. The key amino acid strikingly different from those of the other zinc fingers is highlighted in brown.

de novo protein design based on the zinc finger motif supports the significance of the minimal hydrophobic core formation for proper protein folding. Imperiali and coworkers created a 23-residue peptide folding into the $\beta\beta\alpha$ fold without the aid of Zn(II) (*14*). Similarly, Mayo and coworkers designed a 28-residue peptide with a defined $\beta\beta\alpha$ structure without the metal using a computational design algorithm (*15*). In both studies, the minimal hydrophobic core formed between the helix and the β-hairpin was shown to play a key role in the necessary structure. As the minimal hydrophobic core for the $\beta\beta\alpha$ structure is important, however, the relationships between the stability of the hydrophobic core and DNA binding function have not been reported.

As the design of zinc finger proteins is being explored for many potential applications in various fields of science (*16*−*21*), it is of special interest to study the role of amino acids in the other positions of the helical region in the zinc finger. Recently, we found that the DNA binding ability of the GAGA-DBD depends on the nature of the amino acid in the β-hairpin (*6*). In this study, we focus on the conserved hydrophobic leucine residue located at the fourth position of the recognition helix of the GAGA zinc finger (Figure 1). We designed a set of four peptides by substituting the leucine residue with other aliphatic residues, i.e., Ile, Val, Aib, and Ala, having different degrees of bulkiness and hydrophobicities of the side chains to investigate (i) how the hydrophobic amino acid at helical position 4 (Leu) of the GAGA zinc finger participates in formation of the hydrophobic core and (ii) how the stability of the hydrophobic core plays a critical role in determining the affinity of the GAGA-DBD for the cognate DNA sequence. We envisioned that systematic characterization of these peptides would shed light on the precise role of the Leu side chain in formation of the minimal hydrophobic core and the importance of stabilization of the hydrophobic core on the DNA binding of the GAGA-DBD.

MATERIALS AND METHODS

Peptide Synthesis and Purification. Assembly of the peptide chain was performed on the Rink amide resin by the solid-phase method using a Shimadzu PSSM-8 synthesizer along with the Fmoc strategy with a slightly modified protocol using HATU/TMP as the coupling reagent (*22*). After the assembly, the peptides were cleaved from the resin using a cocktail consisting of 92.5% trifluoroacetic acid, 2.5% water, 2.5% ethanedithiol, and 2.5% triethylsilane for 90 min. The crude peptides were precipitated in ice-cold ether, separated by centrifugation, washed three times with diethyl ether, and finally dissolved in water and lyophilized. The peptide purification was performed using the RP-HPLC system, model L-7100 (Shimadzu Corp.), employing a COSMOSIL RP-C_{18} column (10 mm × 250 mm) (Nacalai Tesque, Inc.) using a linear gradient with acetonitrile and water containing 0.1% trifluoroacetic acid. The purified peptides were characterized by RP-HPLC and laser desorption time-of-flight mass spectrometry (MALDI-TOF): M_{calcd} of 3606.25 Da and $[M - H]_{observed}$ of 3605.23 Da for the wild type, M_{calcd} of 3606.25 Da and $[M - H]_{observed}$ of 3605.76 Da for the Ile mutant, M_{calcd} of 3592.22 Da and $[M - H]_{observed}$ of 3591.53 Da for the Val mutant, M_{calcd} of 3578.19 Da and $[M - H]_{observed}$ of 3577.54 Da for the Aib mutant, and M_{calcd} of 3564.17 Da and $[M - H]_{observed}$ of 3563.70 Da for the Ala mutant).

Ultraviolet−*Visible Absorption Spectroscopy.* The UV−vis absorption spectra were recorded on a Beckman Coulter DU7400 diode array spectrophotometer at 20 °C in Tris-HCl buffer (10 mM, pH 8.0) containing NaCl (50 mM) in a capped 1 cm path length cell. All the presented spectra were normalized by the relationship $\varepsilon = A/lc$, where ε is the extinction coefficient (inverse molar inverse centimeters), l is the path length of the cell (centimeters), and c is the peptide concentration (molar).

Circular Dichroism Spectroscopy. All the circular dichroism experiments were carried out using a JASCO J-720 spectropolarimeter. The spectra were recorded from 195 to 260 nm in the continuous mode with a 1 nm bandwidth, a 1 s response, and a scan speed of 50 nm/min. Each spectrum represents the average of 20 scans at 20 °C in Tris-HCl buffer (10 mM, pH 8.0) containing NaCl (50 mM) in a capped 0.1 cm path length cell under a nitrogen atmosphere. The concentrations of the peptide stock solutions were spectrophotometrically estimated. Thermal denaturation was monitored at 218 and 222 nm, with data acquired at 1 °C intervals between 5 and 85 °C with an equilibration time of 5 min.

Gel Mobility Shift Assay. Each reaction mixture contained Tris-HCl (10 mM, pH 8.0), NaCl (50 mM), $ZnCl_2$ (10 μM), dithiothreitol (1 mM), calf thymus DNA (20 ng/μL), bovine serum albumin (40 ng/μL), Nonidet P-40 (0.05%), glycerol (5%), the FITC-end-labeled substrate DNA fragment (10 nM), and the GAGA peptide (0−1 μM). After incubation at 20 °C for 30 min, the sample was run on an 8% polyacrylamide gel with TB buffer (89 mM Tris-HCl and 89 mM boric acid) at 20 °C. The bands were visualized with a Fluorimager (Molecular Dynamics).

NMR Spectroscopy. The NMR experiments were performed at 20 °C using a Bruker AVANCE500 500 MHz spectrometer. The NMR samples were prepared by dissolving the lyophilized peptide powder in phosphate buffer (20 mM)

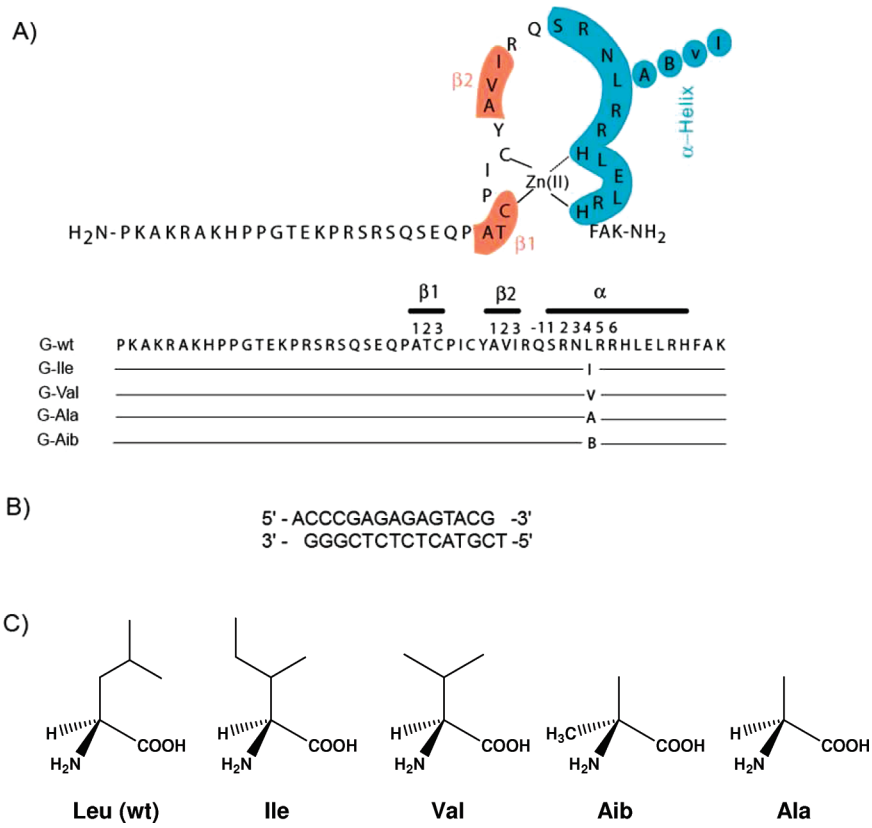

FIGURE 2: (A) Amino acid sequences of GAGA zinc finger mutant peptides. (B) DNA substrates used in this study. (C) Structures of amino acids with various side chain lengths used for point mutations. The positions of the two short β-strands and DNA recognition helix are indicated by the position numbering within them. In the Aib mutant peptide sequence, B denotes the unnatural amino acid α-aminoisobutyric acid.

containing 2,2-dimethyl-2-silapentane-5-sulfonate sodium salt (DSS) as the internal reference for the ^{1}H chemical shifts. The peptide concentration was 300 μM in all the experiments. The pH was adjusted to 7 with concentrated NaOH and HCl. Variable-temperature experiments in the presence of $ZnSO_4$ (1.5 equiv) were conducted in the range between 20 and 50 °C at increments of 5 °C. The H_2O signal was suppressed by a WATERGATE pulse sequence (*23*).

RESULTS AND DISCUSSION

Zinc Coordination of GAGA Zinc Finger Mutants. The peptide−metal coordination chemistry was investigated by UV−vis absorption spectroscopy to examine whether the mutants retain the tetrahedral metal coordination geometry like the wild-type peptide. Since Zn(II) is a spectroscopically silent ion in the visible region of the electromagnetic spectrum because of the d^{10} electronic configuration, the metal coordination of zinc fingers has often been studied using Co(II) as a spectroscopic probe for the zinc site (*24, 25*). The UV−vis spectra of the Co(II) complexes of all the mutants were compared with that of the wild-type peptide in Figure 3A. All the mutants exhibited UV−vis spectra similar to that of the wild-type peptide. The intense absorption bands in the near-UV regions around 316 and 340 nm are indicative of the $S^- \rightarrow$ Co(II) ligand-to-metal charge transfer (LMCT) transition (*26*). The magnitude of the extinction coefficient (ε) at 320 nm reflects the number of thiol-containing ligands coordinated to the metal and averages ∼900−1200 M^{-1} cm^{-1} per S^-−Co(II) bond (*27, 28*). The ε values at 320 nm are around 2000 M^{-1} cm^{-1} for all the peptides, which infers that the peptides use two thiol groups for the coordination with the Co(II). The coordination geometry of the Co(II) in the peptide−metal complex can be estimated on the basis of the ligand-field theory; the optical transitions of a tetrahedral Co(II) species exhibit an intense d−d absorption band in the 625 ± 50 nm region due to the small ligand field stabilization energy (*29*). All the peptides show similar d−d transitions at ∼650 nm, suggesting that Co(II) has a tetrahedral coordination geometry. The titration experiment of these peptides with $CoCl_2$ clearly showed a 1:1 stoichiometry for the peptide−metal complexes (Supporting Information, Figures S1 and S2). In the competition experiments, the bands due to the d−d transition (∼650 nm) observed for the Co(II)−peptide complexes disappeared with the addition of an equivalent amount of the spectroscopically silent Zn(II) (Figure 3B). This observation implies that Zn(II) displaces the Co(II) and occupies the metal binding site of the peptides due to the ligand field stabilization energy difference between Co(II) and Zn(II). This result reveals the peptide−Zn(II) complex is more stable than the peptide−Co(II) complex as shown in other zinc fingers (*30*). Thus, the UV−vis data strongly suggest that replacing Leu with any of the aliphatic amino acids (Ile, Val, Aib, or Ala) at position 4 of the zinc finger helix region does not alter the coordination geometry of the metal binding; i.e., the zinc finger state is similar in all the mutants.

Secondary Structure of GAGA Peptides. Circular dichroism (CD) spectroscopy is a powerful tool for determining the peptide conformation in solution in a fast and reliable manner

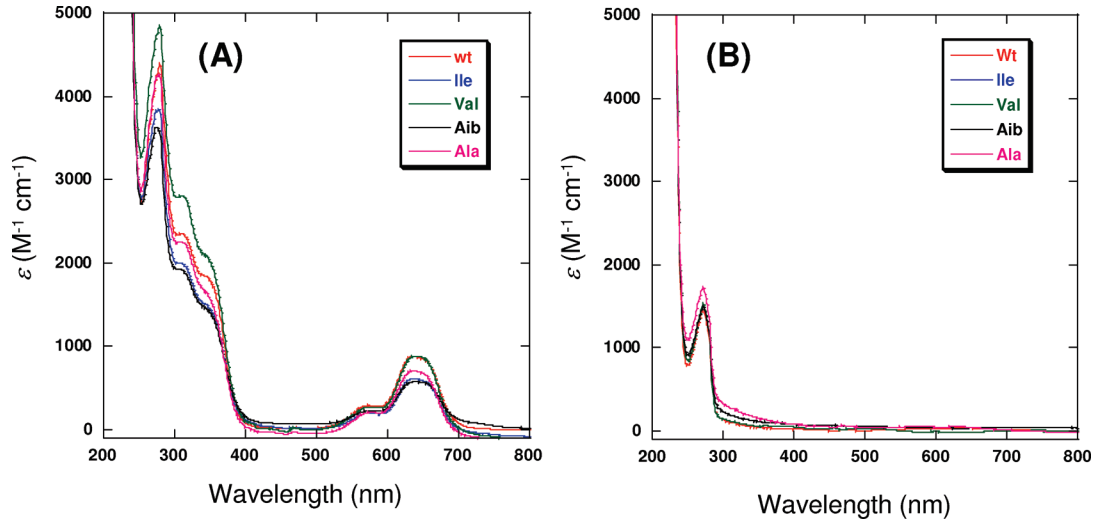

FIGURE 3: UV−vis absorption spectra of (A) Co(II) complexes of GAGA peptides and (B) Co(II) complexes of GAGA peptides in the presence of an equivalent amount of Zn(II).

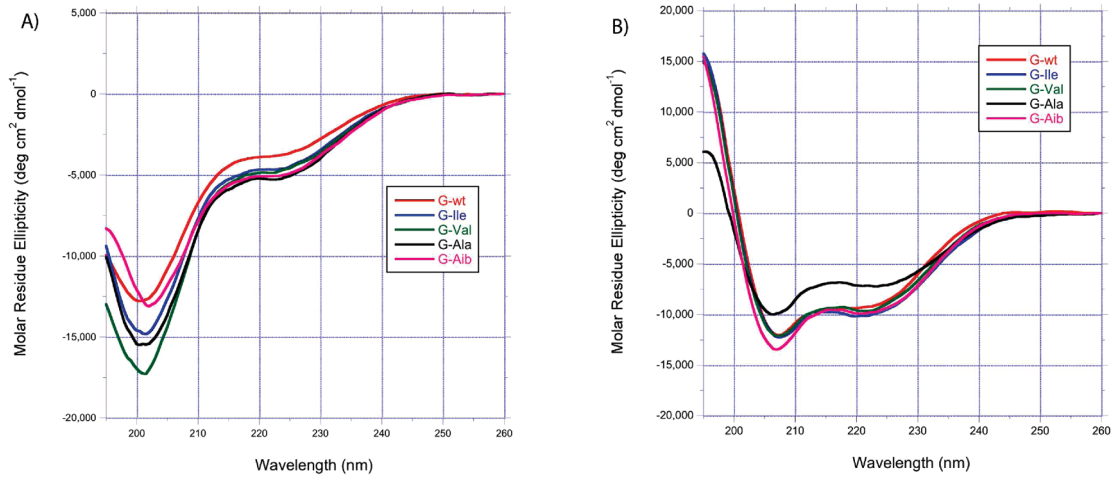

FIGURE 4: Circular dichroism spectra of GAGA mutants (A) in the absence of $ZnCl_2$ and (B) in the presence of $ZnCl_2$.

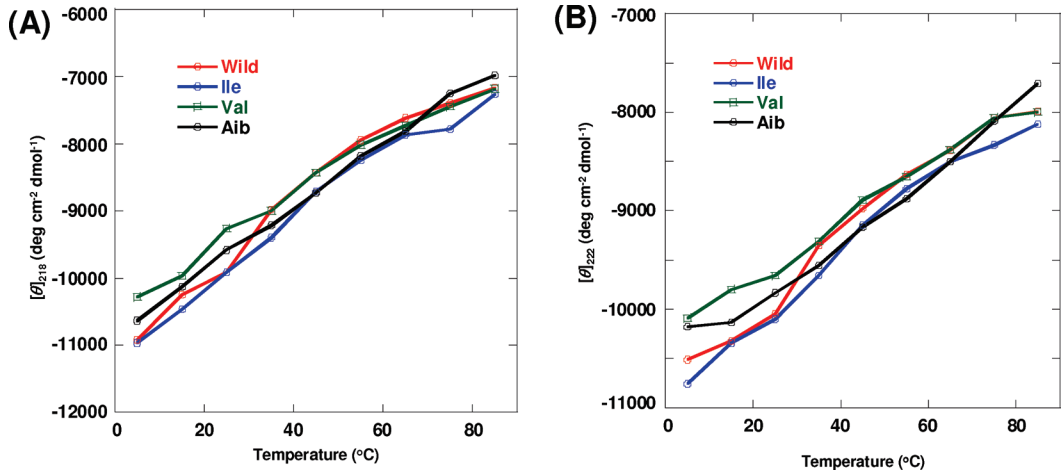

FIGURE 5: Temperature dependence of (A) β-hairpin diagnostic $[\theta]_{218}$ and (B) helix diagnostic $[\theta]_{222}$.

(*31*). Moreover, the CD signature of the zinc finger domain has been well-documented in the literature (*6, 14, 15, 25, 32*). Hence, we used CD to compare the conformational properties of the mutants with those of the wild-type peptide. We have utilized the zinc finger core alone (30 aa) for the CD studies without the N-terminal basic region as it was proposed that the zinc finger core alone is an independent folding motif (*1, 24, 32*−*34*). The CD spectra of the peptides at 20 °C are shown in Figure 4. All the peptides exhibit a negative band near 200 nm ($\pi \rightarrow \pi^*$ electronic transition) and a shoulder around 222 nm (n $\rightarrow \pi^*$ electronic transition) in the absence of $ZnCl_2$, suggesting that the peptides are in a largely random coil conformation with some helical content. Upon addition of $ZnCl_2$, significant changes in the CD spectrum were observed for all the peptides; the intensity significantly increases in the helix diagnostic negative molar

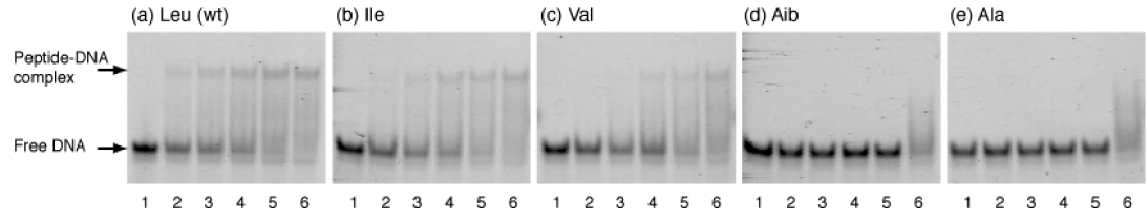

FIGURE 6: Gel mobility shift assays for the peptides to the GAGA DNA sequence. Lanes 1−6 contained 0, 63, 125, 250, 500, and 1000 nM peptide, respectively: (a) wild-type GAGA peptide and (b−e) Ile, Val, Aib, and Ala mutants, respectively.

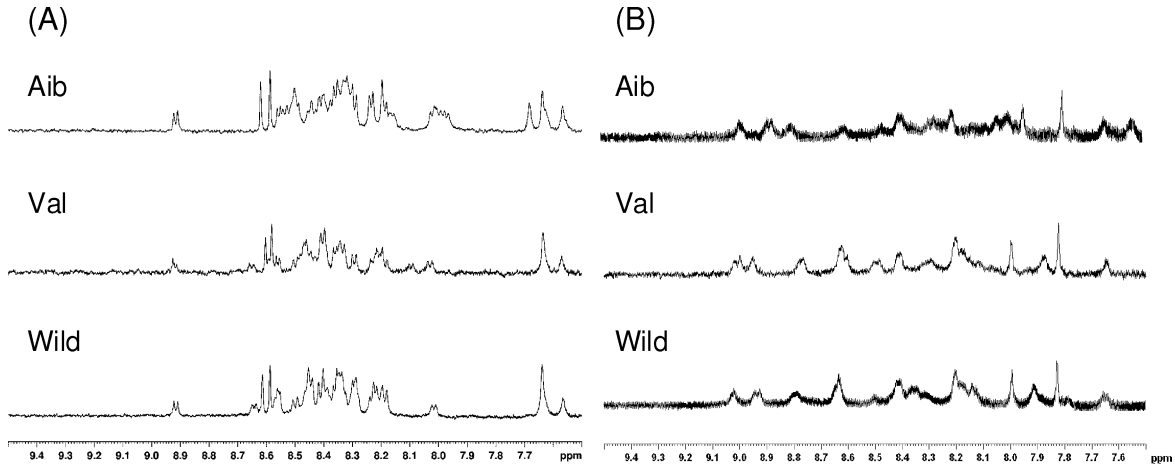

FIGURE 7: ^{1}H NMR spectra of GAGA peptides (wild type, Val, and Aib) in the absence (A) and presence (B) of 1.5 equiv of Zn(II) at 20 °C.

ellipticity at 222 nm and the random coil signature band near 200 nm, with a dramatic reduction in the negative molar ellipticity. These observations indicate that all the peptides fold into the characteristic zinc finger $\beta\beta\alpha$ fold and that the helical content is comparable among all the peptides except for the Ala mutant peptide, suggesting that the Ala mutant peptide has a less folded structure compared to the other peptides. The marginal differences in the CD feature could be due to the minor alteration in the hydrophobic core structure.

An attempt was made to compare the thermal stabilities of all the peptides in the presence of Zn(II) by CD. Since the GAGA zinc finger contains a mixture of secondary structures, we used $[\theta]_{222}$ (helix diagnostic) and $[\theta]_{218}$ (β-hairpin diagnostic) to obtain the thermal melting curve (Figure 5). The full CD spectra of the peptides at different temperatures are given in Figure S3 of the Supporting Information. All the peptides, including the wild-type peptide, exhibited a shallow melting profile, i.e., weakly cooperative folding. Mayo and co-workers showed a similar weak cooperative folding for their de novo designed peptide based on the zinc finger motif (*15*). In summary, the CD results suggest that mutants are able to fold like the wild-type peptide in the presence of $ZnCl_2$, and all the peptides, except for the Ala mutant, exhibit similar thermal stabilities, suggesting that the level of cooperativity of each of these peptides is approximately the same.

Structural Relationship with DNA Binding. The sequence-specific DNA binding abilities of the wild-type GAGA peptide and mutant peptides were evaluated by the gel mobility shift assay. These results are shown in Figure 6. Shifted bands were detected in the DNA binding reactions with the wild-type (Leu), Ile, or Val peptide (Figure 6a−c), indicating that these peptides bind to the GAGA-specific DNA fragment. Though it is difficult to precisely determine the apparent dissociation constants, because of some smearing bands similar to those observed in our previous study on the GAGA zinc fingers (*6*), the DNA binding affinity is progressively reduced as the length of the side chain is reduced [wild type (Leu) > Ile > Val]. The smearing band may be due to some nonspecific interaction with the DNA and/or instability of the peptide−DNA complexes in the gel. Neither the Aib nor Ala mutant peptides produced any detectable shifted bands even at the peptide concentration of 1 μM (Figure 6d,e). It seems that the progressive decrease in the DNA binding affinity reflects the change in the folding structure resulting from mutations introduced into the fourth position of the recognition helix.

As judged from the UV and CD measurements, all the mutants, except for the Ala mutant, with different side chains, do not alter the zinc coordination geometry, and they have almost the same folded structures. Furthermore, the thermal denaturation analysis of the GAGA mutant peptides monitored by CD indicates that the wild type and mutants have similar thermal stabilities. These results indicate that the global changes in the macromolecular structures of the mutant peptides, which are observed as a change in the protein secondary structure content, are very small; i.e., no gross changes in the secondary structures of the GAGA mutant peptides are induced by the substitution of the Leu residue with other aliphatic amino acids. In spite of the slight differences in the overall folding structures among the GAGA mutant peptides, the reason the DNA binding affinity depends on the bulkiness of the substituted aliphatic residue must be explained. Understanding the significant difference in the DNA binding properties between Val and Aib is especially important; that is, the Val mutant can bind to target DNA but not Aib, although both mutants exhibit similar CD features. To estimate how subtle changes in the amino acid side chain length and hydrophobic packing can affect the

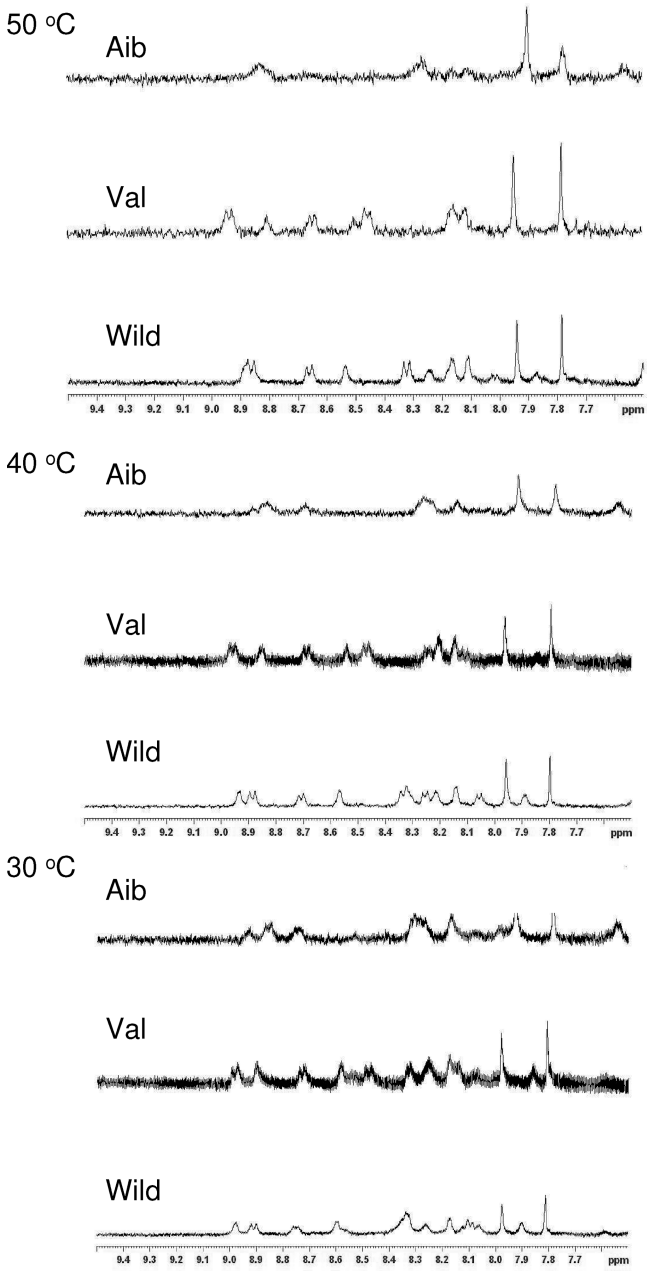

FIGURE 8: Temperature dependence of the ^{1}H NMR spectra of GAGA peptides (wild type, Val, and Aib) in the presence of 1.5 equiv of Zn(II).

binding affinity for the GAGA cognate DNA, we tried to further investigate the microenvironmental change in the mutated GAGA zinc finger domain using the ^{1}H NMR method, because the CD technique normally provides the overall conformation of the peptide in solution and it is generally difficult to obtain precise structural information at the residue level. We expected that the conformational stability, especially the packing of the hydrophobic core, would be more or less affected by the introduction of these mutations and that the mutated zinc finger core domain would shift toward a more molten globule-like state with a reduced level of compaction compared to the wild type. Because proton chemical shifts are very sensitive indicators of the structural integrity of a proton, NMR spectroscopy is reliable for the detection of both the secondary and tertiary structures in folded proteins. In addition, variable-temperature ^{1}H NMR experiments could provide further information about both

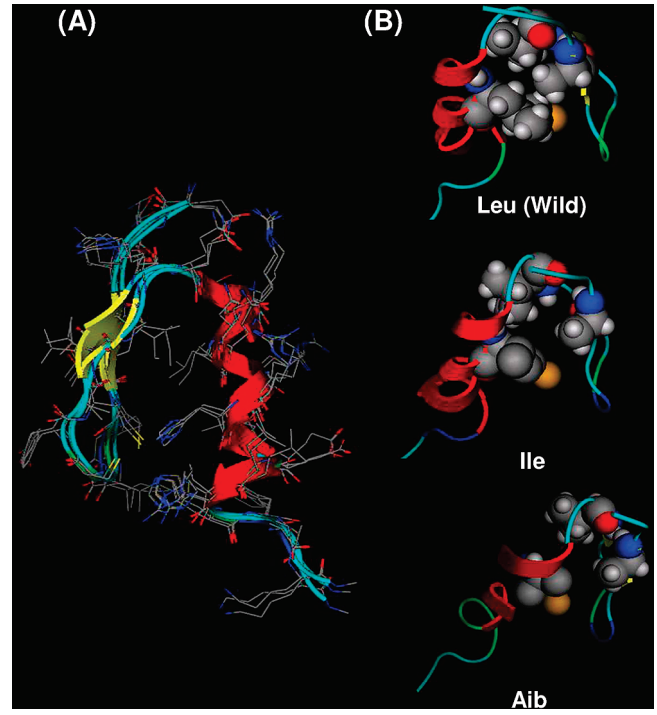

FIGURE 9: Energy-minimized structures of wild-type, Ile, and Aib GAGA peptides using MOE (Chemical Computing Group, Montreal, QC). (A) Superimposed structures of three peptides. (B) Close-up view of the hydrophobic core of the wild type (top), Ile mutant (middle), and Aib mutant (bottom).

the conformational equilibrium and thermal stability in the GAGA zinc finger domains (*33*). The proton NMR spectra of the wild-type, Val, and Aib GAGA peptides recorded at 20 °C in aqueous buffer in the absence and presence of Zn(II) are shown in Figure 7. The NMR spectra of all three peptides in the absence of Zn(II) exhibit the spectral characteristics of the unfolded structures, including less dispersion in the downfield amide proton region (Figure 7A). In contrast, the NMR spectra of the three GAGA peptides in the presence of Zn(II) exhibit a well-dispersed amide region characteristic of the typically folded protein structures as shown in the Figure 7B. Visual inspection of the amide proton region of proton NMR spectra recorded at 20 °C suggests there is a similarity between the peptides.

However, there is a significant change in the spectral features at higher temperatures (Figure 8). The observed changes in the amide proton signals are negligible for the wild-type peptide, slight for the Val peptide, but remarkable in the case of the Aib peptide. In the case of the wild-type peptide, the NMR spectra show an overall good dispersion in the amide region at all temperatures, and there are no significantly observed temperature-dependent chemical shifts in the amide region, indicating that the wild-type peptide and Zn(II) system is in slow exchange on the NMR time scale due to the stable folded structure. At 40 °C, the Val peptide yielded a spectrum with even less dispersion in the amide region (especially in the range of 8.0−8.5 ppm) compared to that of the wild-type peptide. This could be due to the loss of the tight packing of the $\beta\beta\alpha$ fold; i.e., the stability of the folded structure of the Val mutant is slightly lower than that of the wild type. On the other hand, the NMR spectrum of the Aib peptide clearly shows a weaker dispersion in the downfield amide region compared to the wild-type and Val peptide even at 30 °C. The magnitudes

of the amide proton signals of the Aib peptide decreased at 40 °C and disappeared at 50 °C. No evidence of any precipitation was observed at the higher temperature. These data suggested that the motion of the backbone structure of the Aib peptide becomes almost the same as the NMR time scale with an increase in temperature and that the structural stability of the Aib mutant is obviously lower than those of the wild-type and Val peptides. In contrast to the CD measurement results, the variable-temperature NMR experiments clearly showed the differences in the stability between the Val and Aib mutants, and the importance of the bulkiness of the conserved aliphatic residue for the formation of the well-packed minimal hydrophobic core and proper ternary structure. In addition, the hydrophobic core stabilization, which plays a crucial role in the formation of the stable folded structure, apparently influences the DNA binding function of the GAGA zinc finger.

To further examine the effects of the bulkiness of the hydrophobic amino acid residue on (i) the overall backbone structure and (ii) the formation and stability of the hydrophobic core, the peptides were subjected to an energy minimization calculation using a standard protocol available in the Molecular Operating Environment (MOE) system. The NMR structure (Protein Data Bank entry 1YUJ) was used as a starting structure for the calculations with the appropriate mutations at the position of interest (*5*). The resultant final energy-minimized structures are overlaid in Figure 9A. The root-mean-square deviation (rmsd) between the structures is 1.3866 Å when all the atoms are considered. However, if only the backbone atoms are considered, the rmsd is less than 1 Å. This result suggests that the overall conformation of the mutants is similar to that of the wild-type peptide as shown by the CD measurements. On the other hand, the observation of a reduced DNA binding affinity as the bulkiness of the side chain is reduced suggests that the bulkiness of the side chain at this position is important for promoting the optimal hydrophobic core. Figure 9B shows the close-up views of the hydrophobic core of the GAGA-DBD. The tight packing of the minimal hydrophobic core, which is necessary for forming the compact $\beta\beta\alpha$ fold of the zinc finger domain, gradually becomes relaxed as the length of the side chain is reduced. Thus, the loss of DNA binding for the Aib mutant is possibly due to the bulkiness (side chain length) not being sufficient for formation of a stable hydrophobic core.

In conclusion, substitution of the consensus Leu residue located at the fourth position of the recognition helix of the GAGA-DBD retains zinc finger folding, except for the Ala mutant, but the specific DNA binding activity decreases as the side chain length of the amino acid decreases. This study demonstrates that the bulkiness of the conserved Leu residue is important in the formation of the well-packed minimal hydrophobic core and proper ternary structure, and the stability of the hydrophobic core apparently influences the DNA binding function of the GAGA zinc finger.

SUPPORTING INFORMATION AVAILABLE

UV−vis spectra of peptides with increasing concentrations of $CoCl_2$ and CD spectra of peptides in the presence of $ZnCl_2$ at different temperatures. This material is available free of charge via the Internet at http://pubs.acs.org.

REFERENCES

1. Iuchi, S. (2001) Three classes of C_2H_2 zinc finger proteins. *Cell. Mol. Life Sci. 58*, 625–635.
2. Tupler, R., Perini, G., and Green, M. R. (2001) Expressing the human genome. *Nature 409*, 832–833.
3. Granok, H., Leibovitch, B. A., Shaffer, C. D., and Elgin, S. C. R. (1995) Chromatin: Ga-ga over GAGA factor. *Curr. Biol. 5*, 238–241.
4. Pedone, P. V., Ghirlando, R., Clore, G. M., Gronenborn, A. M., Felsenfeld, G., and Omichinski, J. (1996) The single Cys_2-His_2 zinc finger domain of the GAGA protein flanked by basic residues is sufficient for high-affinity specific DNA binding. *Proc. Natl. Acad. Sci. U.S.A. 93*, 2822–2826.
5. Omichinski, J. G., Pedone, P. V., Felsenfeld, G., Gronenborn, A. M., and Clore, G. M. (1997) The solution structure of a specific GAGA factor-DNA complex reveals a modular binding mode. *Nat. Struct. Biol. 4*, 122–132.
6. Dhanasekaran, M., Negi, S., Imanishi, M., and Sugiura, Y. (2007) DNA-binding ability of GAGA zinc finger depends on the nature of amino acids present in the β-hairpin. *Biochemistry 46*, 7506–7513.
7. Fairall, L., Schwabe, J. W. R., Chapman, L., Finch, J. T., and Rhodes, D. (1993) The crystal structure of a two zinc-finger peptide reveals an extension to the rules of zinc-finger/DNA recognition. *Nature 366*, 483–487.
8. Pavletich, N. P., and Pabo, C. O. (1991) Zinc finger-DNA recognition: Crystal structure of a Zif268-DNA complex at 2.1 Å. *Science 252*, 809–816.
9. Pavletich, N. P., and Pabo, C. O. (1993) Crystal structure of a five-finger GLI-DNA complex: New perspectives on zinc fingers. *Science 261*, 1701–1707.
10. Urnov, F. D., Miller, J. C., Lee, Y. L., Beausejour, C. M., Rock, J. M., and Augustus, S. (2005) Highly efficient endogenous human gene correction using designed zinc-finger nucleases. *Nature 435*, 646–651.
11. Segal, D. J., Crotty, J. W., Bhakta, M. S., Barbas, C. F., III, and Horton, N. C. (2006) Structure of Aart, a designed six-finger zinc finger peptide, bound to DNA. *J. Mol. Biol. 363*, 405–421.
12. Vonderfecht, T. R., Schroyer, D. C., Schenck, B. L., McDonough, V. M., and Pikaart, M. J. (2008) Substitution of DNA-contacting amino acids with functional variants in the Gata-1 zinc finger: A structurally and phylogenetically guided mutagenesis. *Biochem. Biophys. Res. Commun. 369*, 1052–1056.
13. Imperiali, B., and Ottesen, J. J. (1998) Design strategies for the construction of independently folded polypeptide motifs. *Biopolymers 47*, 23–29.
14. Struthers, M. D., Cheng, R. P., and Imperiali, B. (1996) Economy in protein design: Evolution of a metal-independent $\beta\beta\alpha$ motif based on the zinc finger domains. *J. Am. Chem. Soc. 118*, 3073–3081.
15. Dahiyat, B. I., and Mayo, S. L. (1997) De novo protein design: Fully automated sequence selection. *Science 278*, 82–87.
16. Negi, S., Imanishi, M., Matsumoto, M., and Sugiura, Y. (2008) New redesigned zinc-finger proteins: Design strategy and its application. *Chem.—Eur. J. 14*, 3236–3249.
17. Wu, J., Kandavelou, K., and Chandrasegaran, S. (2007) Custom-designed zinc finger nucleases: What is next? *Cell. Mol. Life Sci. 64*, 2933–2944.
18. Dhanasekaran, M., Negi, S., and Sugiura, Y. (2006) Designer zinc finger proteins: Tools for artificial DNA-binding functional proteins. *Acc. Chem. Res. 39*, 45–52.
19. Klug, A. (2005) Towards therapeutic applications of engineered zinc finger proteins. *FEBS Lett. 579*, 892–894.
20. Blancafort, P., Segal, D. J., and Barbas, C. F. (2004) Designing transcription factor architectures for drug-discovery. *Mol. Pharmacol. 66*, 1361–1371.
21. Jamieson, A. C., Miller, J. C., and Pabo, C. O. (2003) Drug discovery with engineered zinc-finger proteins. *Nat. Rev. Drug Discovery 2*, 361–368.
22. Nokihara, K., Nagawa, Y., Hong, S.-P., and Nakanishi, H. (1997) Efficient solid-phase synthesis of a large peptide by a single coupling protocol with a single HPLC purification step. *Lett. Pept. Sci. 4*, 141–146.
23. Piotto, M., Saudek, V., and Sklenár, V. (1992) Gradient-tailored excitation for single-quantum NMR spectroscopy of aqueous solutions. *J. Biomol. NMR. 2*, 661–665.
24. Frankel, A. D., Berg, J. M., and Pabo, C. O. (1987) Metal-dependent folding of a single zinc finger from transcriptional IIIA. *Proc. Natl. Acad. Sci. U.S.A. 84*, 4841–4845.

25. Nomura, A., and Sugiura, Y. (2002) Contribution of individual zinc ligands to metal binding and peptide folding of zinc finger peptides. *Inorg. Chem. 41*, 3693–3698.
26. Giedroc, D. P., Keating, K. M., Williams, K. R., Konigsberg, W. H., and Coleman, J. E. (1986) Gene 32 protein, the single-stranded DNA binding protein from bacteriophage T4, is a zinc metalloprotein. *Proc. Natl. Acad. Sci. U.S.A. 83*, 8452–8456.
27. May, S. W., and Kuo, J.-Y. (1978) Preparation and properties of cobalt(II) rubredoxin. *Biochemistry 17*, 3333–3338.
28. Vašák, M., Kägi, J. H. R., Holmquist, B., and Vallee, B. L. (1981) Spectral studies of cobalt(II)- and nickel(II)-metallothionein. *Biochemistry 20*, 6659–6664.
29. Bertini, I., and Luchinat, C. (1984) High spin cobalt(II) as a probe for the investigation of metalloproteins. *Adv. Inorg. Biochem. 6*, 71–111.
30. Berg, J. M., and Merkle, D. L. (1989) On the metal ion specificity of "zinc finger" proteins. *J. Am. Chem. Soc. 111*, 3759–3761.
31. Woody, R. W. (1995) Circular dichroism. *Methods Enzymol. 246*, 34–71.
32. Parraga, G., Horvath, S. J., Eisen, A., Taylor, W. E., Hood, L., Young, E. T., and Klevit, R. E. (1988) Zinc-dependent structure of a single-finger domain of yeast ADR1. *Science 241*, 1489–1492.
33. Lachenmann, M. J., Ladbury, J. E., Philips, N. B., Narayana, N., Qian, X., and Weiss, M. A. (2002) The hidden thermodynamics of a zinc finger. *J. Mol. Biol. 316*, 969–989.
34. Lee, M. S., Gippert, G. P., Soman, K. V., Case, D. A., and Wright, P. E. (1989) Three-dimensional solution structure of a single zinc finger DNA-binding domain. *Science 245*, 635–637.

BI801306D